# Identification of Formyl Kynurenine Formamidase and Kynurenine Aminotransferase from *Saccharomyces cerevisiae* Using Crystallographic, Bioinformatic and Biochemical Evidence‡

Mark Wogulis, Erin R. Chew, Paul D. Donohoue, and David K. Wilson*

*Section of Molecular and Cellular Biology, University of California, Davis, California 95616*

*Received June 13, 2007; Revised Manuscript Received November 21, 2007*

ABSTRACT: The essential enzymatic cofactor $NAD^+$ can be synthesized in many eukaryotes, including *Saccharomyces cerevisiae* and mammals, using tryptophan as a starting material. Metabolites along the pathway or on branches have important biological functions. For example, kynurenic acid can act as an NMDA antagonist, thereby functioning as a neuroprotectant in a wide range of pathological states. *N*-Formyl kynurenine formamidase (FKF) catalyzes the second step of the $NAD^+$ biosynthetic pathway by hydrolyzing *N*-formyl kynurenine to produce kynurenine and formate. The *S. cerevisiae* FKF had been reported to be a pyridoxal phosphate-dependent enzyme encoded by BNA3. We used combined crystallographic, bioinformatic and biochemical methods to demonstrate that Bna3p is not an FKF but rather is most likely the yeast kynurenine aminotransferase, which converts kynurenine to kynurenic acid. Additionally, we identify YDR428C, a yeast ORF coding for an $\alpha/\beta$ hydrolase with no previously assigned function, as the FKF. We predicted its function based on our interpretation of prior structural genomics results and on its sequence homology to known FKFs. Biochemical, bioinformatics, genetic and *in vivo* metabolite data derived from LC−MS demonstrate that YDR428C, which we have designated BNA7, is the yeast FKF.

Nicotinamide adenine dinucleotide ($NAD^+$)[1] has a widespread role as an essential enzymatic redox cofactor found in all branches of life. Additionally, it has been found to participate in functions such as deacetylation and DNA ligation (*1*−*4*) (reviewed in (*5*)). These reactions regulate important biological processes such as aging, transcriptional regulation and tumorigenesis (*4*, *6*, *7*). Animals and *Saccharomyces cerevisiae* are known to produce $NAD^+$ via *de novo* synthesis, with tryptophan as a starting material. This pathway converges with a salvage pathway that produces nicotinate mononucleotide (NaMN), which the *de novo* pathway also produces. In this salvage pathway, nicotinate phosphoribosyltransferase, which in *S. cerevisiae* is encoded by NPT1, converts nicotinate (Na) into NaMN, which is then converted into $NAD^+$ (Figure 1) (*6*, *8*).

The *de novo* synthesis of $NAD^+$ generates metabolic intermediates that are either biologically active themselves or that serve as starting materials to produce other biologically active metabolites (*9*). For example, kynurenic acid (KA) production in humans has generated considerable interest due to its activity as an NMDA antagonist and its consequent value in protecting against neuronal damage from stroke (*10*). KA has also been implicated in regulation of blood pressure and glucose metabolism. Metabolites of the *de novo* pathway have been implicated in a range of human diseases, including Huntington's disease, hypoxic brain damage, schizophrenia, and tumor growth, to name just a few (*11*). Understanding the enzymatic control of this pathway is therefore of considerable interest.

Formylkynurenine formamidase (FKF) catalyzes the second step of the pathway by hydrolyzing the formyl moiety of *N*-formyl kynurenine (NFK) to produce kynurenine (KYN) and formate (Figure 1). Kynurenine is a branchpoint and can serve as a substrate for either kynurenine aminotransferase (KAT) or kynurenine monooxygenase (KMO, BNA4 in *Saccharomyces cerevisiae*). KMO hydroxylates KYN to form 3-hydroxykynurenine, which is the next intermediate in the *de novo* $NAD^+$ biosynthetic pathway. Alternatively, KAT converts the amino acid moiety of kynurenine into an α-keto acid (*8*) which then spontaneously cyclizes to form kynurenic acid (KA). KAT is a PLP dependent enzyme that utilizes a "ping-pong bi−bi" reaction mechanism (*12*). In this mechanism a primary amine of the kynurenine is replaced by a ketone, leaving behind the enzyme in its PMP form. The PLP form of the enzyme is regenerated by a second reaction in which the amino group is transferred to an α-keto acid to produce an amino acid and the enzyme in its PLP form (Figure 2) (*13*). KATs are able to use a wide variety of α-keto acids and amino acids as cosubstrates in this reaction, and it is not clear which ones predominate *in vivo* (*14*−*18*).

Previous work identified six candidate open reading frames encoding the *Saccharomyces cerevisiae de novo* $NAD^+$ biosynthesis pathway based on sequence homology with

‡ The coordinates have been deposited into the Protein Data Bank as PDB ID 3B46.

* Corresponding author. Section of Molecular and Cellular Biology, One Shields Ave., University of California, Davis, CA 95616. Phone: (530)752-1136. Fax: (530)752-3085. E-mail: dave@alanine.ucdavis.edu.

[1] Abbreviations: aeKAT, *Aedes aegypti* kynurenine aminotransferase; FKF, formylkynurenine formamidase; hKAT-I, human kynurenine aminotransferase I; KA, kynurenic acid; KAT, kynurenine aminotransferase; KYN, kynurenine; $NAD^+$, nicotinamide adenine dinucleotide; NFK, *N*-formylkynurenine; rnKAT-I, rat kynurenine aminotransferase I; ttGlnAT, Thermus thermophilus HB8 glutamine:phenylpyruvate aminotransferase;

10.1021/bi701172v CCC: $40.75 
Published on Web 01/19/2008

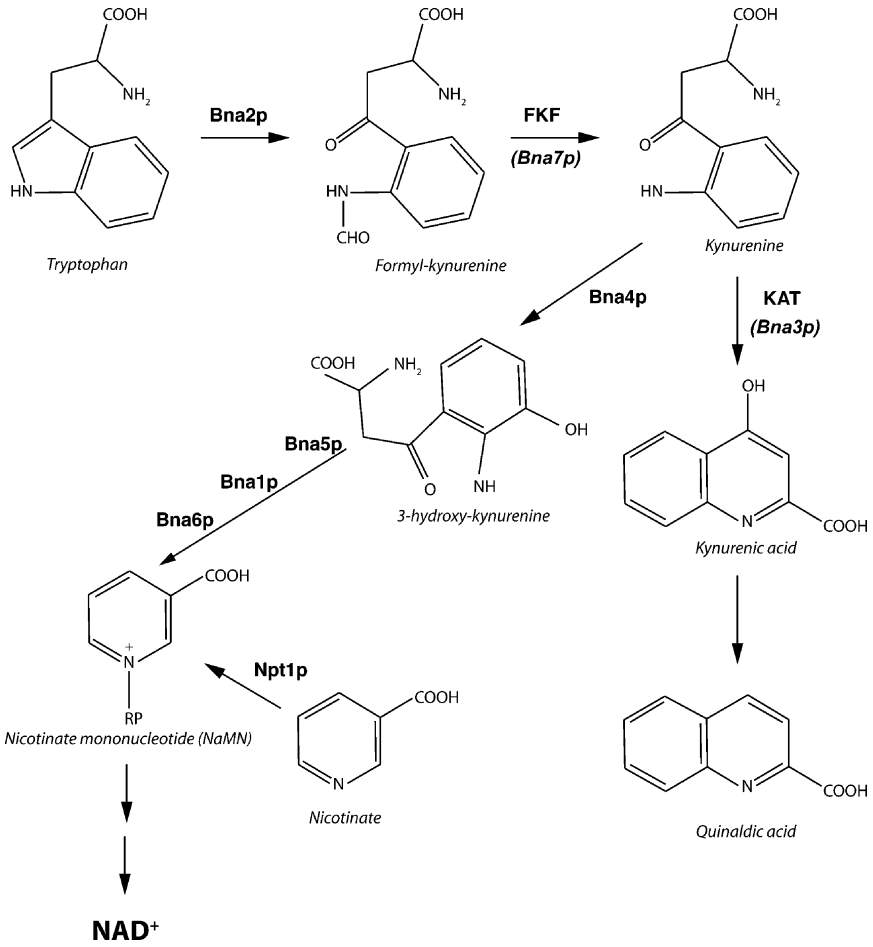


FIGURE 1: Schematic of the $NAD^+$ biosynthesis pathway. This schematic is greatly simplified and omits most of the branching pathways and many of the catalytic steps. Bna2p is trytophan-2,3-doxygenase. Bna4 is kynurenine monooxygenase.

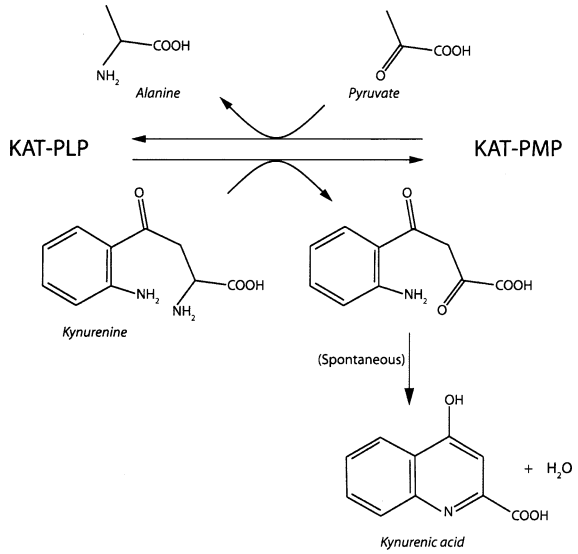


FIGURE 2: KAT reaction mechanism. All KATs discussed in this work are able to utilize a variety of α-keto acids in order to convert KAT in the PMP form to KAT in the PLP form.

known mammalian enzymes, and they were designated BNA1−6 (biosynthesis of nicotinic acid) (Figure 1) (*8*, *19*). Yeast strains were created in which each putative $NAD^+$ biosynthetic enzyme and the nicotinate salvage enzyme nicotinate phosphoribosyltransferase (NPT1) were deleted. These double deletions resulted in a synthetic lethal phenotype for five of the six genes. Single deletions of each of these enzymes resulted in nicotinate auxotrophs in five of the six candidates. In both cases, BNA3 (YJL060W) which was identified as the FKF in the pathway did not exhibit the expected phenotype (*8*). Furthermore, experiments designed to understand the genetic control of $NAD^+$ biosynthesis showed that, when the BNA pathway was up-regulated, all BNA genes except for BNA3 were up-regulated together (*20*). For example, the transcription factor Sum1p recruits the $NAD^+$ dependent deacetylase Hst1p. In these experiments, Hst1p appeared to regulate *de novo* $NAD^+$ biosynthesis. In a *sum1*Δ strain expression levels of BNA2 increased 14.1-fold, BNA4 11.7-fold, BNA5 4.6-fold, BNA1 3.9-fold and BNA6 1.9-fold, while BNA3 levels were unchanged. Together, these data raise the question as to whether BNA3 is indeed the yeast FKF.

In this work, we present the crystal structure of Bna3p and show by primary sequence and structural homology, as well as by biochemical evidence, that it is not the FKF but, rather, a KAT. Furthermore, we demonstrate that the YDR428C gene product, which had previously been characterized in a structural genomics screen as an α/β-hydrolase protein of unknown function (*21*), is in fact the yeast FKF. We designate YDR428C as BNA7, and demonstrate its function using primary sequence homology and biochemical, genetic and structural evidence.

## RESULTS

*Bna3p Has Primary Sequence Homology to Known KATs but Not FKFs.* Panozzo et al. (*8*) had identified BNA3 as a

Table 1: Selected Kynurenine Aminotransferases from a BLASTP Search of Nonredundant Protein Sequences Using BNA3p Amino Acid Sequence as a Query

| organism | accession code | % identity | % similar | *E*-value |
|---|---|---|---|---|
| *Aspergillus fumigatus* | XP_447929 | 53 | 74 | $9 \times 10^{-125}$ |
| *Dictyostelium discoideum* | XP_637331 | 36 | 56 | $3 \times 10^{-68}$ |
| *Aedes aegypti* | EAT44194 | 34 | 51 | $5 \times 10^{-64}$ |
| *Trypanosoma brucei* | XP_823403 | 35 | 54 | $6 \times 10^{-63}$ |
| *Rattus norvegicus* | AAF06837 | 35 | 53 | $2 \times 10^{-61}$ |
| *Homo sapiens* | Q16773 | 35 | 53 | $2 \times 10^{-61}$ |

formyl transferase rather than as a formyl hydrolase. The murine FKF has been identified, and based on sequence analysis and mutagenesis experiments it appears to be an $\alpha/\beta$ hydrolase fold enzyme (*22*, *23*). Bna3p is not an $\alpha/\beta$ hydrolase fold enzyme, however. Rather its primary sequence identifies it as a PLP dependent amino transferase. To identify homologous proteins in order to understand its function, we ran a BLASTP search (*24*) of the Bna3p sequence against a database of nonredundant protein sequences. In the top 100 hits (with *E*-values ranging from 0 for an unnamed protein product from *Candida galbrata*, accession code XP_447929, to $6 \times 10^{-58}$ for hypothetical protein OsJ_028446 from *Oryza sativa*) the only functions assigned in the names are kynurenine aminotransferase, kynurenine oxoglutarate transaminase, cysteine conjugate beta lyase (one of the original names for what is now called kynurenine aminotransferase I) or simply transaminase or aminotransferase. Among the proteins identified as kynurenine aminotransferases are those from *Aspergillus fumigatus*, *Dictyostelium discoideum*, *Aedes aegypti*, *Trypanosoma brucei*, *Rattus norvegicus*, and *Homo sapiens* (Table 1). The top two matches of a BLASTP search of the Protein Data Bank are the above-mentioned KATs from *Homo sapiens* (PDB id 1W7N (*25*)) and *Aedes aegypti* (PDB id 1YIY (*26*)). The third highest match (34% identical, 53% similar, *E*-value $6 \times 10^{-57}$) is *Thermus thermophilus* HB8 glutamine: phenylpyruvate aminotransferase (ttGlnAT) (PDB id 1V2D (*16*)), which has been shown to efficiently catalyze the transamination of KYN (*27*). This primary sequence homology to known KATs clearly demonstrates that Bna3p should be classified as a KAT rather than an FKF.

*Bna3p Has Structural Homology to Known Kynurenine Aminotransferases.* To test the hypothesis that BNA3 encodes an aminotransferase, we obtained diffraction data from single crystals of Bna3p and attempted molecular replacement with human kynurenine aminotransferase I (hKAT-I) as a search model. Using this method, we have determined the crystal structure of Bna3p at 2.0 Å resolution (Table 2). The crystal contained one dimer per asymmetric unit, and the final, refined model contains 849 amino acids (including the catalytic internal aldimine between PLP and Lys271) and 242 waters (Figure 3). The model had an $R_{cryst}$ of 22.7% and an $R_{free}$ of 27.1%. Ramachandran statistics show only one residue (Phe303) per monomer subunit in the disallowed region. The homologous position in the hKAT-I structure was also in the disallowed region, and the electron density at this position was quite good. Additionally, there was only one residue (Thr357) per monomer in a generously allowed region, and the electron density was sufficiently good to preclude a more favorable positioning. The overall main-chain and side-chain geometry was good, being within or better than typical values for this resolution, according to analysis by the program PROCHECK. The rmsd between 364 manually identified homologous $C_\alpha$s of Bna3p and hKAT-I was 1.5 Å.

The overall fold is typical for an aminotransferase subgroup I. This fold contains a large and a small domain, along with an N-terminal arm (*25*). The biological unit consists of a dimer with two active sites, each lying near the dimer interface. Residues from both monomer subunits contribute to each active site (Figure 3).

The first helix of the small domain (residues 34−45) is mobile, and its movement is important for the activity of the enzyme (*12*, *28*). The significance of this movement of the helix may explain why the rat KAT-I (rnKAT-I) with a Glu61Gly missense mutation is a slower enzyme than the wild-type enzyme (Figure 4). This mutation is at the end, or "hinge" of this first helix. Since this residue is distant from the active site and is on the surface of the enzyme, the mutation is presumed to affect the movement of the helix (*12*). In hKAT-I, *Aedes aegypti* KAT (aeKAT) and ttGlnAT there is a short 2 amino acid loop between the first helix and the first beta strand of the small subunit. This loop is even structurally conserved in an hKAT-II homologue from *Pyrococcus horikoshii* (1X0M) (*29*) which is only distantly related (23% identical, 41% similar, *E*-value $2 \times 10^{-5}$) to Bna3p compared to hKAT-I, aeKAT and ttGlnAT. In contrast, Bna3p has a 9 residue loop in that position, much of which was disordered in this crystal structure (Figure 4).

The ability to solve the Bna3p crystal structure using hKAT-I as a molecular replacement search model demonstrates the close structural similarity between Bna3p and hKAT-I. To determine the closest known structural homologue, we used the solved structure of Bna3p to do a DALI search of representative members of structural families in the PDB (*30*). Using residues 55 through 444 of the Bna3p structure (i.e., leaving out the mobile first helix of the small domain) the closest match is the aeKAT (1YIY, which is the PMP form of the enzyme). In fact, using DaliLite (*31*) pairwise comparisons with the PLP forms of the enzymes, aeKAT, hKAT-I and ttGln:AT are all structurally highly homologous to Bna3p (Table 3).

*Bna3p Binding Pocket Is Homologous to Those of Other KATs.* Despite the significant difference in the hinge region, the active site and binding pocket residues of Bna3p are highly conserved as compared to hKAT-I, aeKAT, and ttGlnAT (Figure 4). A model for the binding of kynurenine to the active site of ttGlnAT has been generated based on three crystal structures of ttGlnAT (one unliganded, one with 3-phenylpropionate bound in the active site, and one with $\alpha$-keto-$\gamma$-methylthiobutarate bound in the active site) (*16*). We have used this proposed orientation of substrate in ttGlnAT to model kynurenine in the active site of Bna3p (Figure 3D). The good fit of kynurenine in the active site of Bna3p, as well as the conservation in other KATs of many residues that interact with the substrate in this model, is consistent with this protein being a yeast KAT. Of the 7 residues from one protomer (Trp35, Gly62, Asn125, Phe149, Asp150, Gln151, Arg420) and 1 from the other protomer (Phe303*) that contact the substrate in this model, 4 are absolutely conserved and 2 are conserved as aromatic residues in the three other structurally determined proteins

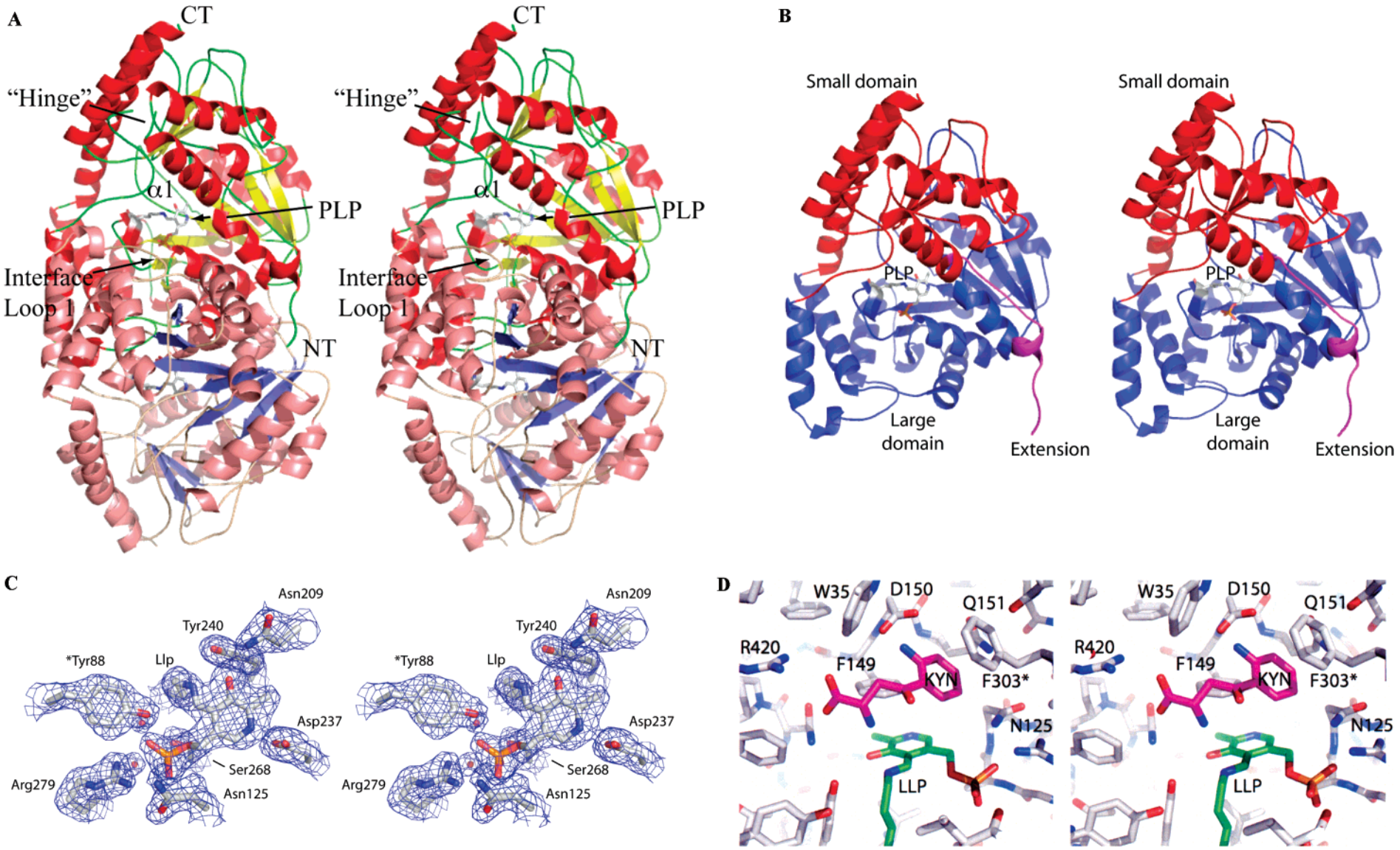


FIGURE 3: Stereoview of Bna3p. (A) Bna3p homodimer. The figure is color coded by secondary structure, with each monomer of the homodimer colored differently. "CT" indicates the C-terminus of one monomer and "NT" the N-terminus of the same monomer. The first helix of the small domain is labeled "α1." (B) Monomer subunit of Bna3p homodimer color coded by domain. Large domain is shown in blue, the small domain in red and the N-terminal extension in magenta. (C) Side chains of Bna3p active site with their electron density map. The map is a sigma weighted $2F_o - F_c$ electron density map contoured at 1$\delta$. (D) Model of KYN bound to Bna3p binding pocket. All residues that KYN are predicted to interact with are shown, with the exception of Gly62, which was left out for clarity.

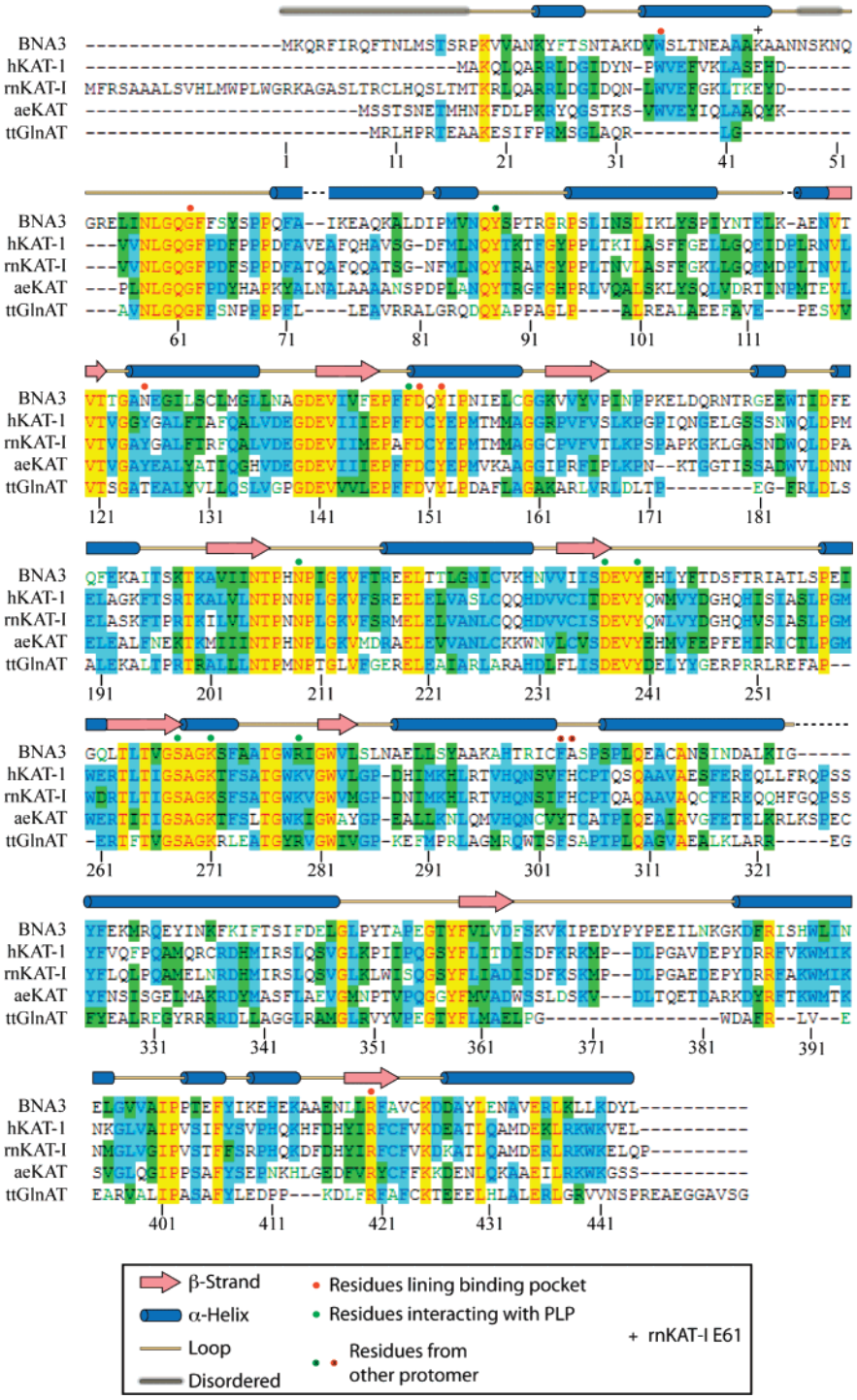


FIGURE 4: Primary sequence alignment of Bna3p, hKAT-I, aeKAT, and ttGlnAT. Secondary structure of Bna3p is indicated above the alignment. Numbering is for Bna3p. Absolutely conserved residues are shown in red type with yellow background. Residues conserved in at least 3 of the 5 are shown in blue type with light blue background. Blocks of residues of similar kind are shown in black type with green background. Residues involved in PLP or substrate binding are designated with green and red dots respectively. The location of the E61G hinge mutation in rats is also identified.

with KAT activity (Figure 4). Only 2 of the 8 are not conserved.

The amino acid moiety binding pocket portion of the model is fairly certain because of the multiple structures that have inhibitor or substrate present with either a carboxylic acid or amino acid moiety. In this portion of the model, Arg420 makes a salt bridge with the carboxylic acid of the substrate. This highly conserved residue helps orient the amine in close proximity to PLP to position it so that it forms the internal aldimine intermediate. A conserved glycine at position 62 is within van der Waals distance of the substrate amino acid group. This residue is part of a conserved NLGQ**G**F (residues 58−63) sequence that helps shape this portion of the binding pocket (Figure 4).

The positioning of the remainder of the substrate molecule is more speculative. However, the crystal structures with inhibitors and substrates provide a reasonable basis for the model. Phe303* stacks against the KYN aryl ring, as does

Table 2: Data Collection and Structure Refinement Statistics for PLP-Bound Bna3p[a]

| | |
|---|---|
| **Data Collection Statistics** | |
| wavelength (Å) | 0.97944 |
| resolution (Å) (highest shell) | 50−1.96 (2.03−1.96) |
| reflections (observed/unique) | 214,880/60,609 |
| completeness (%) | 98.6(93.6) |
| $I/\sigma(I)$ | 36.9 (4.7) |
| $R_{merge}$ | 0.065 (0.255) |
| **Refinement Statistics** | |
| resolution (Å) | 28.8−2.0 |
| $R_{cryst}$ (%) | 22.7 |
| $R_{free}$ (%) | 27.1 |
| rmsd bond lengths (Å) | 0.0095 |
| rmsd bond angles (deg) | 1.59 |
| DPI | 0.19 |
| Ramachandran plot | |
| % in most favorable regions | 91.5 |
| % in additional allowed regions | 8.0 |
| % in generously allowed regions | 0.3 |
| % in disallowed regions | 0.3 |

[a] Parentheses indicate values for the high resolution shell.

Table 3: Results of DaliLite Pairwise Comparisons to Three Enzymes with KAT Activity, Using Residues 55−444 of Chain A of Bna3p Crystal Structure

| source organism | PDB ID | *Z*-score | res. aligned | rmsd (Å) |
|---|---|---|---|---|
| *Homo sapiens* | 1W7L | 52.2 | 397 | 1.7 |
| *Aedes aegypti* | 1YIY | 52.6 | 380 | 1.6 |
| *Thermus thermophilus* | 1V2D | 47.9 | 343 | 1.3 |

Phe149, which in turn also stacks against the PLP aromatic ring. Phe149 is conserved in these three crystal structures with KAT activity (as well as in rnKAT-I), and the stacking interaction between Phe303* and KYN is also conserved (though the residue is a tyrosine in aeKAT). (Figure 4) The significance of this phenylalanine for substrate binding in the hKAT-I structure has previously been noted (*25*). Asp150 is conserved in all four proteins, and in this model it forms a hydrogen bond with the KYN aryl amine, as it does in the model of KYN bound to ttGlnAT (*16*). In the Bna3p crystal structure (unliganded), the Asp150 side chain makes no direct hydrogen bond contacts with any other residues, suggesting that the conservation is functional for substrate binding rather than structural. Trp35 is the most difficult residue to model accurately because it is on the mobile small domain first helix. Trp35 is conserved as a tryptophan in hKAT-I and aeKAT, though it is a phenylalanine in ttGlnAT. However, in the hKAT-I structure with L-phenylalanine as a substrate in the active site, the hKAT-I tryptophan in this position (Trp18) clearly contacts the substrate and is an important part of the substrate binding pocket.

In the model, kynurenine also makes van der Waals contacts with the side chain of Gln151 (whose amide moiety points away from the substrate). Gln151 is not conserved among these structures (it is a cysteine in hKAT-I and aeKAT, and a valine in ttGlnAT), but the contact is weak. Asn125 is not conserved in hKAT-I and aeKAT (where it is a Tyr), but neither is it conserved in ttGlnAT (where it is a Thr). Ala304* in Bna3p does not contact the modeled substrate, though the corresponding residue in hKAT-I (His279*) contacts the L-phenylalanine substrate. However, this residue is not conserved as a His in either aeKAT or ttGlnAT.

Overall, the structural and primary sequence homology of the Bna3p active site to other known KATs further supports its designation as a KAT.

*Bna3p Shows Kynurenine Amino Transferase Activity in Vitro.* In order to measure the activity of Bna3p toward KYN, we developed a continuous assay in which an increase in $OD_{285}$ was used to observe the formation of KA. hKAT-I and aeKAT are both able to catalyze formation of KA using a variety of different α-keto acids as oxygen donors in the reaction (*17*, *18*). For both enzymes, many of the α-keto acids showed substrate inhibition at low mM concentrations. The concentration at which the substrate inhibition was seen as well as the velocity of the enzymes with a given concentration of KYN varied between the two enzymes. We attempted to measure the $k_{cat}$ and $K_m$ of Bna3p with KYN as a substrate and pyruvate as the oxygen donor. Unfortunately, KYN showed substrate inhibition at concentrations over 5 mM (Supplemental Figure 1, Supporting Information), and pyruvate showed substrate inhibition at 10 mM, as did α-ketoglutarate (data not shown). α-Ketobutyrate showed substrate inhibition down to 2 mM, though the velocity of the enzyme with 4 mM kynurenine was faster with α-ketobutyrate as a cosubstrate than with α-ketoglutarate or pyruvate. We were unable to convincingly fit a standard Michaelis−Menten curve to our data, even when adding an inhibition term to the denominator of the equation. An apparent $k_{cat}$ and $K_m$ for the human enzyme were generated using 16 mM α-ketobutyrate as an oxygen donor in the reaction (*18*). In their conditions, they did not observe substrate inhibition. This gave an apparent $k_{cat}$ of 201 ± 19 $min^{-1}$. Since the $K_m$ was measured to be 4.7 ± 0.4 mM, the reaction rate at 4.7 mM is 100 $min^{-1}$. The rate of Bna3p at 37 °C using 5 mM pyruvate and 4 mM KYN as cosubstrates was 1 $min^{-1}$, 2 orders of magnitude slower than the human enzyme (or than aeKAT, which has a comparable $k_{cat}$ and $K_m$ to hKAT-I) measured at 45 °C. Although Bna3p has lower activity than do hKAT-I and aeKAT, it is clearly capable of catalyzing the formation of KA from KYN, consistent with its characterization as a KAT.

*YDR428C Has Homology to the Murine Formylkynurenine Formamidase.* The classification of Bna3p as a yeast KAT raised the question of which protein functions as the FKF. A WU-BLAST search (*32*) of the SGD database using the murine FKF sequence identifies three possible yeast homologues. One (Cct6p, *E*-value 0.998) is a subunit of the cytosolic chaperonin Cct ring complex (*33*), and thus is unlikely to act as an FKF. The other two (YDR428C, *E*-value 0.993 and YJR098C, *E*-value 0.81) are from uncharacterized ORFs. YDR428C and the murine FKF are roughly the same size as each other (261 vs 305 amino acids, respectively) while YJR098C is much larger (655 amino acids). Furthermore, a pairwise sequence alignment of the proteins shows that YDR428C is 11% identical and 22% similar to the murine FKF, while YJR098C is 5% identical and 11% similar to the murine FKF. In this alignment, the residues around the catalytic serine align between YDR428C and the murine FKF (with sequences of GH**S**VGA vs GH**S**AGA, respectively) while YJR098C does not show homology in this area. Significantly, both the murine FKF and YDR428C have the canonical Gly-X-Nuc-X-Gly motif (where Nuc is a nucleophile, which is a serine for both of these enzymes) that is found in most α/β hydrolase fold enzymes (*34*).

YJR098C lacks this motif entirely, bringing into question whether this enzyme is even an α/β hydrolase. Additionally, a structural genomics effort has yielded the crystal structure of YDR428C (PDB accession 1VKH) (*21*), and it demonstrates common features of an α/β hydrolase fold enzyme, such as the conserved arrangement of a Ser-Asp-His catalytic triad, the "nucleophile elbow," and the ordering of the beta strands and alpha helices.

Because of the size similarities, the better primary sequence alignment, and the structural proof that it is an α/β hydrolase enzyme, we identified YDR428C as the most likely yeast FKF. Work described below supports this hypothesis and has accordingly led to the name BNA7.

*Analysis of the Bna7p Structure Suggests That It Is a Formylkynurenine Formamidase.* The crystal structure of Bna7p reveals a hydrophobic substrate binding cleft lined by the following residues: Ala39, Trp40, Val111, Ile153, Leu156, Leu159, Tyr166, Phe169, Leu213 and Leu214. NFK can be modeled into this cleft such that the hydrophobic side of the aryl moiety faces into this hydrophobic patch (Figure 5). The exact fit of the substrate is difficult to predict accurately because residues 155 to 181 form a lid subdomain, such as those seen in many lipases (*21*). In the lipases, these lids move upon substrate binding and it is difficult to predict what structural changes may occur to accommodate the substrate. Nevertheless, the hydrophobic cleft in this structure suggests an orientation of an NFK substrate in which the aryl group fits into the cleft.

The *N*-formyl moiety must be oriented toward the attacking nucleophile (Ser110) for the hydrolysis reaction to proceed. The hydrolytic mechanism of an α/β hydrolase enzyme proceeds via the creation of an unstable oxyanion, which is stabilized by an oxyanion hole made up of backbone amide nitrogens. In the case of Bna7p, the nitrogen atoms of Gly38, Asn39 and Val111 make up the oxyanion hole. For NFK, the oxyanion is formed from the aldehyde. Therefore, if the aryl moiety is oriented toward the hydrophobic cleft, the formation of the tetrahedral intermediate will force the formyl hydrogen to point toward a small pocket formed by the side chains of Asp42, Asp49, Asn244, and Tyr247 (Figure 5C). This small pocket would hinder the hydrolysis of larger or hydrophobic acid moieties of the amide. The structure of Bna7p active site and catalytic residues are therefore consistent with a function as the yeast FKF.

*Biochemical Evidence That Bna7p Is a Formylkynurenine Formamidase.* We have cloned BNA7 from yeast genomic DNA into the pTYB2 expression vector. Bna7p was expressed and affinity purified. It was tested for FKF activity using NFK as a substrate and was found to have significant activity. $k_{cat}$ of BNA7p is 161 $s^{-1}$, and $K_m$ is 0.18 ± 0.02 mM (Figure 6). Therefore, the specificity constant $k_{cat}/K_m$ is $8.9 \times 10^5$ $s^{-1}$ $M^{-1}$. This high catalytic efficiency is consistent with NFK being a native substrate for this enzyme. The kinetic parameters of this enzyme were compared to published values for the recombinantly expressed, affinity purified murine enzyme (*23*), and they are similar. The $K_m$ values of the murine (0.18 ± 0.02 mM) and yeast (0.18 ± 0.02 mM) enzymes were indistinguishable. The $V_{max}$ value reported for the murine enzyme was given without noting the concentration of enzyme used, and therefore cannot be directly compared to the value reported here. However, the velocity of the reactions can be roughly compared in two ways, using their specific activity measurement of purified recombinant enzyme at 0.45 mM NFK, which is 24 $s^{-1}$ (reported as 42 μmol/min/mg) for wild-type enzyme. The specific activity of Bna7p at the similar concentration of 0.5 mM NFK is 112 $s^{-1}$, which is roughly 4.7 times faster than the murine enzyme. Alternatively, their specific activity measurement and substrate concentration can be used to solve the Michaelis−Menten equation. The $k_{cat}$ calculated this way is 34 $s^{-1}$, again roughly 4.7 times slower than Bna7p. Clearly, Bna7p is an even more efficient enzyme for the hydrolysis of NFK than is the murine FKF. Conversely, recombinantly expressed, purified Bna3p shows no measurable aryl formamidase activity *in vitro*, even at 7,000 times the protein concentration of Bna7p in this assay. These *in vitro* activities are consistent with the hypothesis that Bna7p, rather than Bna3p, is the FKF in yeast.

*Bna7 Is a Formylkynurenine Formamidase in Vivo.* The BNA7 and NPT1 double knockout has been examined in a global genetic analysis of synthetic fitness or lethality defect interactions screen (*35*), and has been determined to have a slow growth phenotype. This screen identified *bna1, 4, 5* and *6* as synthetic lethal with *npt1*Δ, consistent with Panozzo's results (*8*). An additional 7 genes were also identified as being synthetic lethal in a double knockout with NPT1, though none of them could reasonably function as FKFs. In addition to YDR428C (BNA7), 37 other genes were identified as having a synthetic fitness/synthetic lethal phenotype. This provides genetic interaction evidence consistent with a role for BNA7 in the $NAD^+$ biosynthetic pathway. For more direct evidence of *in vivo* function, *S. cerevisiae* BNA3 and BNA7 knockout strains were obtained. We have extracted metabolites from these two strains, along with the corresponding parent strain using the cold methanol extraction method developed by Maharjan and Ferenci (*36*). The extracts have been examined by LC−MS for the presence of NFK, KYN, KA, quinaldic acid (dehydroxylated KA, which is produced directly from KA), and 3-hydroxykynurenine (the product of Bna5p, which competes with KAT for KYN). The expectation is that *bna7*Δ strain will show an increase in NFK levels, but a decrease in all other metabolites measured (since all of these metabolites are downstream of Bna7p). If BNA3 is a KAT, only KA and quinaldic acid should show reduced levels in the *bna3*Δ strain, while NFK should remain unchanged, and KYN and the other tested metabolites should be unaffected or increased. Unfortunately, the only metabolite that was consistently and reproducibly measurable using our growth, extraction and detection systems was NFK, the Bna7p substrate. Even with NFK, we were only able to measure it in the *bna7*Δ strain and not in the parental or the *bna3*Δ strain. However, the level of NFK in the *bna7*Δ strain was nearly 100-fold higher than the limits of detection of the assay (data not shown). While we could draw no conclusions about the *in vivo* function of BNA3, the extremely robust accumulation of NFK in the absence of its putative enzyme (Bna7p) strongly indicates that Bna7p is the yeast FKF.

*bna7*Δ *Strain Shows a Slow Growth Phenotype in the Absence of Exogenous Nicotinate.* In the absence of *de novo* $NAD^+$ biosynthesis, yeast should require an exogenous source of the cofactor. This can be provided as a precursor in the form of nicotinate, which is converted to NaMN by

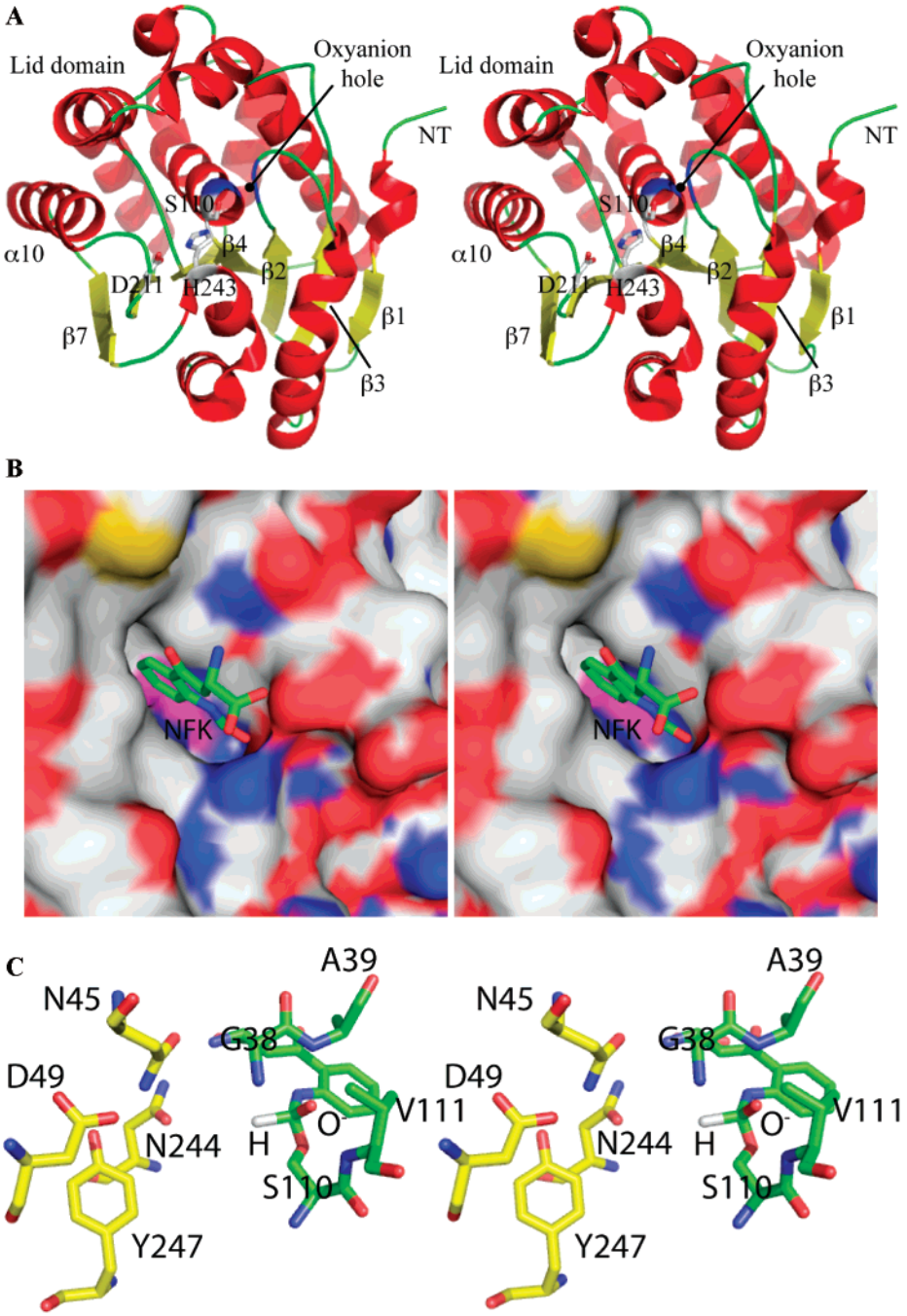


FIGURE 5: Stereoview of Bna7p crystal structure. (A) Cartoon representation of the overall structure. The catalytic triad is labeled and shown in stick representation. The location of the oxyanion hole is indicated in blue. The N-terminus is indicated by "NT." The lid domain consists of three α-helices. NFK is expected to be oriented such that the hydrophobic aryl ring points toward the lid domain, and the formyl moiety sits just on the opposite side of oxyanion hole from the lid domain. (B) Surface representation of Bna7 with a model of NFK placed in the binding cleft as described in text. The catalytic serine is colored magenta and sits at the bottom of the cleft. (C) Model of Bna3p-NFK tetrahedral intermediate. The NFK-Ser110 tetrahedral intermediate is shown with carbons in green and is labeled "S110". The backbone nitrogen atoms of Gly38, Ala39 and Val111 make up the oxyanion hole. The carbon atoms of these residues are also colored green. The side chains of Asn45, Asp49, Asn244, and Tyr247 make a small pocket that precludes a large or nonpolar group attached to the substrate amide nitrogen from fitting into the active site. The carbons in these residues are colored yellow.

Npt1p and then into $NAD^+$ (Figure 1). The nutritional requirement is not absolute for all of the BNA pathway genes. For example, *bna1*Δ strains had a modest slow growth phenotype in the absence of nicotinate, while *bna2*Δ, *bna5*Δ, and *bna6*Δ had no growth in the absence of exogenous nicotinate. Deletions of all four of these genes were synthetic lethal with NPT1 deletion (*8*). Because BNA7 deletion was not synthetic lethal, but rather synthetic slow growth with NPT1 deletion (*35*), we expected a less severe phenotype of *bna7*Δ than is seen in *bna1*Δ when grown in the absence of nicotinate. Growth rates of *bna3*Δ, *bna7*Δ and parent strains were followed by measuring $OD_{600}$ over time. Of the three strains, only the *bna7*Δ strain showed a significant difference in growth in the absence as compared to in the presence of nicotinate. (Figure 7). The doubling time of the *bna7*Δ strain in the absence of exogenous nicotinate was 45% longer than in the presence of nicotinate. The doubling times of the *bna7*Δ strain in the presence of nicotinate, and wild type

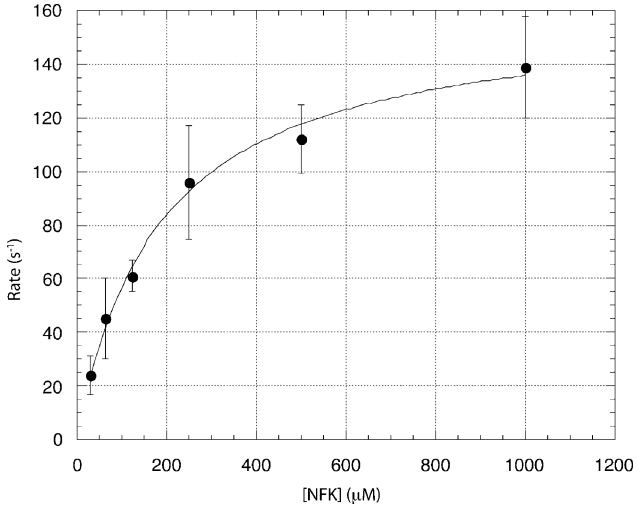


FIGURE 6: Formylkynurenine formamidase activity for Bna7p. The average of six experiments was plotted. The error bars represent ± standard deviation. The Michaelis−Menten equation was fit to the data. $R^2$ for the fit was 0.99.

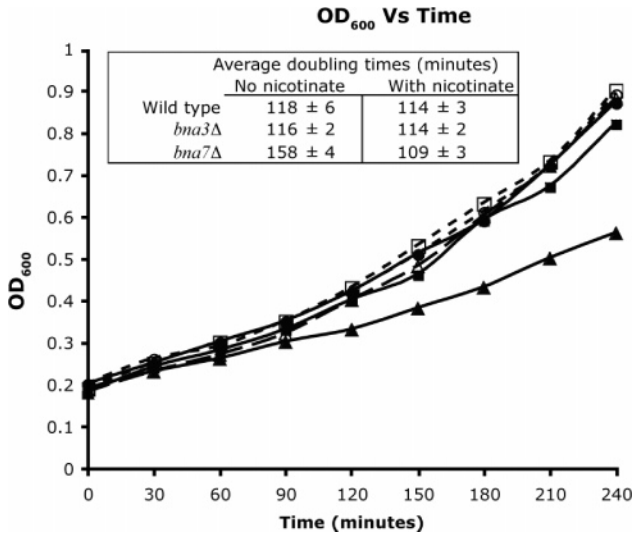


FIGURE 7: Typical growth curves of wild type, *bna3*Δ, and *bna7*Δ strains either with or without nicotinate added to defined media. With nicotinate: Wild type (□), *bna3*Δ (○), *bna7*Δ (△). Without nicotinate: Wild type (■), *bna3*Δ (●), *bna7*Δ (▲). Inset: Average ± standard deviation of calculated doubling times from three independent experiments.

and *bna3*Δ strains in either the presence or absence of nicotinate, were statistically indistinguishable from each other. This provides further evidence that BNA7 works in the *de novo* $NAD^+$ biosynthesis pathway.

## DISCUSSION

Several lines of evidence demonstrate that the Bna7p is the *S. cerevisiae* FKF. First, it has sufficient homology to the identified murine form that it could be identified by a sequence homology search. Second, the structural features of the enzyme are consistent with its chemical function (hydrolase), and the binding cleft appears to favor binding a substrate with the structural and chemical features of NFK. Third, *in vitro* biochemical assays demonstrate that the enzyme can act on NFK as a substrate, and that it has a high specificity constant of $8.9 \times 10^5\ s^{-1}\ M^{-1}$. Fourth, BNA7 deletion genetically interacts with NPT1 deletion. Fifth, metabolic analysis on a *bna7*Δ strain demonstrates a large buildup of the NFK substrate relative to the parent strain. Sixth, Δ*bna7* strain has a nicotinate dependent slow-growth phenotype.

Previous identification of the murine FKF relied on the ability to purify the activity from homogenates. However, many α/β hydrolase enzymes, such as rabbit carboxyesterase, are able to hydrolyze a fairly wide range of substrates (*37*). Thus, an α/β hydrolase that is present in high concentration or that is particularly robust to purification protocols could appear to be the FKF even if that is not its *in vivo* function. Further evidence that the murine FKF is the enzyme that catalyzes hydrolysis of NFK *in vivo* was provided by experiments in which inhibitors of FKF were given to mice, and were shown to alter the levels of tryptophan metabolites (*23*). However, inhibitors of α/β hydrolases can have broad activity (*38*), and it can be difficult to distinguish *in vivo* which enzyme is being targeted, particularly if two hydrolases are able to hydrolyze the same substrate. Thus, using a metabolomic approach combined with genetic manipulation provides a more specific and targeted way of assigning *in vivo* function to an enzyme.

To date, no other crystal structure of an FKF has been determined. Having the crystal structure of Bna7p provides some insight into the likely structure of the mammalian FKFs. Based on primary sequence alignments, the murine FKF has a 57 amino acid N-terminal extension relative to Bna7p. Though the overall primary sequence alignment is poor, the residues around the oxyanion hole (residues 36−40) are conserved between the two structures. This sequence is at the end of β-strand 2, which is sandwiched between and parallel to strands 3 and 4. This arrangement of strand "*n*" sandwiched between parallel strands "*n* + 1" and "*n* + 2" is a nearly universal feature of the α/β hydrolase family. An additional antiparallel "*n* − 1" strand next to strand "*n* + 1" is also quite common (*34*). Thus, the murine FKF almost certainly has this structural arrangement as well, and the additional 57 residues most likely extend the N-terminus of the protein, as indicated by the primary sequence alignment.

There are 100 residues between the yeast catalytic serine and the catalytic aspartate. This stretch includes the 26 residue lid subdomain of this structure. The corresponding murine portion is 16 residues shorter, and it is therefore unclear to what extent the lid domain is conserved.

Both FKFs have 31 residues between the catalytic aspartate and the catalytic histidine. Therefore, the aspartate−helix−strand−histidine arrangement found in the yeast FKF is also likely to be found in the murine FKF. The helix in this arrangement is helix 10 of the structure, and the strand is strand 7 (Figure 5A). The crystal structure of Bna7p shows a noncrystallographic dimer with a large buried interface. Such an interface is also seen in *Bacillus subtilis* brefeldin A esterase, which is the most similar structurally characterized homologue to Bna7p (*21*). In the interface, strand 7 from one monomer binds to strand 7 from the other monomer, making a single, 14 strand β sheet core to the dimer. Helix 10 also forms part of the dimer interface. It is therefore likely that the murine FKF shares this feature.

While the assignment of *in vivo* function to Bna7p is quite clear, the *in vivo* function of Bna3p is less certain. Primary sequence homology as well as structural homology strongly

argues in favor of Bna3p being the yeast KAT. In particular, the binding pocket residues of Bna3p show high structural homology to those found in hKAT-I, aeKAT and ttGlnAT. Different KATs show preferences for different α-keto acid cosubstrates, however. Since these cosubstrates must bind in the same pocket as KYN, some variation in the binding pocket is to be expected between the different KATs (Figure 4). Furthermore, there is some speculation that KAT enzymes have multiple functions. In fact, hKAT-I was initially identified as glutamine transaminase K and also had cysteine conjugate β-lyase activity. It is capable of transaminating multiple amino acids, and hKAT-I has a higher specificity constant for glutamine transamination than it does for kynurenine transamination (*18*). Multiple functions for Bna3p are suggested by the observation that *bna3*Δ is synthetic lethal with a deletion of the spindle checkpoint gene *MAD1*, while *bna7*Δ is not, even though both mutations should lead to a loss of the ability to produce KA (*39*). On the other hand, this difference in synthetic lethality may be a reflection in the timing of KA production rather than in its presence or absence *per se*. There is evidence, in fact, that Bna3p expression is cell cycle related (*18*), and this might account for the difference rather than differing functions.

Further complicating the issue is the existence of multiple KAT enzymes. Mammals have two KAT enzymes that produce KA in the brain. These are referred to as KAT-I and KAT-II, and they are structurally distinct PLP dependent enzymes (*29*, *40*). The relative activity of these two enzymes in brain extracts varies with the region examined (*41*). Despite the existence of KAT-II activity, a mutation in KAT-I leads to a kynurenic acid sensitive phenotype, indicating a physiologically important role for KAT-I (*12*). It appears that *S. cerevisiae* also has at least two KAT enzymes. Aro9 has been identified as the yeast aromatic aminotransferase II, but it was shown to have a broad range of substrate specificity and was able to catalyze the conversion of kynurenine to kynurenic acid in cell extracts (*42*). Aro9p is 23% identical and 40% similar to hKAT-II, and a BLASTP search of the *S. cerevisiae* genome using the hKAT-II protein sequence returns Aro9p (*E*-value $6 \times 10^{-37}$) and Aro8p (*E*-value $2 \times 10^{-49}$) (25% identical and 40% similar to hKAT-II) as the two closest homologues of hKAT-II. Kynurenine aminotransferase activity in cell extracts was reduced by 96% in *aro9* and by 15% in *aro8* strains versus wild type. There was no measurable KAT activity in the double mutant (*aro8 aro9*) strain (*42*). This argues against BNA3 as functioning as a KAT *in vivo*. However, it is important to note that *in vitro* activity in extracts may not reflect actual activity *in vivo*. Concentrations of competing substrates and inhibitors are different in extracts than *in vivo*. Furthermore, aromatic aminotransferase activity varied with growth conditions (*42*), as do expression levels of BNA3 (*43*). It is therefore not clear which enzymes have biologically significant KAT activity *in vivo*, and under which environmental conditions the activity is found.

In addition to primary sequence and structural homology, biochemical experiments provide evidence that Bna3p is a yeast KAT. The enzyme is clearly capable of converting KYN to KA. Activity of recombinant hKAT-I and aeKAT was measured at 45 °C, where it is presumably more active than at a lower temperature. Bna3p was not stable in these conditions, and so the activity was measured at 37 °C. Further complicating the comparison is the differing levels of cosubstrate inhibition in the different forms of the enzymes. These conditions make a direct comparison of KAT activity between Bna3p and hKAT-I and aeKAT problematic, and the enzyme may not be quite as slow relative to the other two enzymes as the data seem to suggest. Nevertheless, it is clear that Bna3p is significantly slower (or possibly has a much higher $K_m$) than hKAT-I and aeKAT. That Bna3p appears to be a much less efficient enzyme for transamination of KYN might indicate that KYN is not the native substrate of Bna3p. However, it appears that the inefficiency of the enzyme is not restricted to KYN. Changing the cosubstrate from pyruvate to α-ketobutyrate significantly increases the velocity of the reaction. This suggests that the rate-limiting step in the conversion of KYN to KA in the presence of pyruvate is not the KYN to KA reaction, but the regeneration of the PLP form of the enzyme using pyruvate. This, in turn, suggests that Bna3p is more generally a slow enzyme and it is not just slow due to the inefficient use of KYN as a substrate. It is interesting to note that a single mutation in the "hinge region" of N-terminal helix of the small domain significantly slowed rat KAT-I activity. The missense mutation is from a glutamate to a glycine, which would presumably increase flexibility in the region. This region is conserved among the other KAT enzymes but is significantly different in Bna3p. In Bna3p there are an extra 7 residues in this region, and several of those residues are disordered, with the remainder only poorly ordered, suggesting more flexibility in this region than is found in the more catalytically active structures. This region is connected to the first α helix of the small domain. Because movement in this domain is important for catalytic function, it is reasonable to presume that the change in the "hinge region" may affect the catalytic efficiency of Bna3p.

In summary, we demonstrate that Bna3p is clearly not the yeast FKF. Instead, it should be classified as a KAT based on strong sequence and structural homology. Biochemical evidence in the form of *in vitro* activity assays also demonstrates (weak) KAT activity that is consistent with the Bna3p structure. Furthermore, our data clearly demonstrate that Bna7p is the yeast FKF. We provide sequence similarity evidence, structural evidence, biochemical evidence and genetic evidence that all strongly support this conclusion. A crystal structure for this ORF already existed from a structural genomics screen, but the specific function of the gene was unknown. Therefore by identifying the function of this ORF, we have identified the first crystal structure of an FKF.

## MATERIALS AND METHODS

*Materials.* KYN, 3-hydroxykynurenine, pyruvate, α-ketobutyric acid and α-ketoglutarate were from Sigma. Quinaldic acid was from Alfa Aesar. KA was from Acros Organics. Formic acid, acetic anhydride, ethyl ether, and acetonitrile were from Fisher. Trifluoroacetic acid was from J. T. Baker. Methanol was from EM Science. Ethanol was from Gold Shield Chemical Company. Yeast strains were purchased from Open Biosystems. *bna3*Δ, catalog number YSC1021-549480, clone ID 11363, and *bna7*Δ, catalog number YSC1021-547375, clone ID 14264. Both strains were MATα mating type. Parent strain used to generate the knockouts was a gift from the lab of Dr. Sean Burgess.

*Synthesis of N-Formylkynurenine.* NFK was synthesized essentially as described previously (*44*). We were unable to purify the product by recrystallization with ethanol as had been done in the original method. Instead, the filtered, ethanol washed precipitate was dried and LC−MS analysis indicated that, in addition to the NFK, *N*-acetyl kynurenine (NAK) was also made, and constituted a significant portion (over 30%) of the entire material. The mixture of NFK and NAK was dissolved in water and separated by HPLC (see below), and the resulting fractions were snap frozen in an ethanol/dry ice bath and the solvent (trifluoroacetic acid, water and acetonitrile) was removed with an unheated SpeedVac. The purified NFK was dissolved in water, and its concentration was determined by enzymatically converting a diluted sample to KYN and then determining concentration by OD, using KYN as a standard. Full conversion to KYN was verified by HPLC (see below). The NFK solutions were greater than 95% pure, and the product's identity as NFK was confirmed by LC−MS.

*HPLC Analysis of Kynurenine and Its Derivatives.* Unbuffered aqueous solutions of KYN or its *N*-formyl and *N*-acetyl derivatives were loaded on a Sephasil Peptide C18 12 $\mu$m ST 4.6/250 (Amersham) column using an AKTA P-903 HPLC system with an AKTA UV-900 detector, INV 907 injection valve, M925 mixer and PV908 switch, and a Frac900 fraction collector. Buffer A was 0.1% aqueous TFA, and buffer B was acetonitrile (ACN) alone. The flow rate was 4 mL/min. 50 to 100 $\mu$L of sample was loaded on the column with 500 $\mu$L of buffer A, and the column washed with 2 column volumes of buffer A. The compound was then eluted using a 0% to 30% gradient of buffer B over 10 column volumes, with the compounds eluting at around 13% acetonitrile. This gave baseline separation between the *N*-acetyl and *N*-formyl derivatives when loading up to 50 $\mu$L of 40 mM mixture. The retention time of 100 $\mu$L of a 500 $\mu$M KYN stock was 27.7 min, while the retention times of the *N*-formyl and *N*-acetyl derivatives were 28.7 min and 30.5 min respectively. When purifying NFK, 0.2 mL fractions of the NFK peak were collected up to baseline. These were pooled and then dried as described above. Purity of purified NFK was determined by integrating NFK and KYN peaks using UNICORN data analysis and absorbance at 260 nm.

*Cloning of BNA3 and BNA7.* Genes were PCR amplified from genomic DNA using primers (BNA7 forward primer, 5′-gctagtgcatatgtcaaataccgtaagagcc-3′; BNA7 reverse primer, 5′- actgcccgggacaaatattgtcaaaaatata-3′; BNA3 forward primer, 5′-gctagtgcatatgaaacaacgattcattcgt-3′; BNA3 reverse primer, 5′-actgcccgggtaagtagtccttgagtagttt-3′) with an *Nde*I restriction site added to the 5′ end of the forward primer, and a *Xma*I restriction site added to the 3′ end of the reverse primer (which contained the stop codon for BNA3). PCR product and pTYB vectors (pTYB12 for BNA3 and pTYB2 for BNA7) were cut with the *Nde*I and *Xma*I restriction enzymes, and the PCR products were ligated into the appropriate pTYB vector. TOP10 *Escherichia coli* cells were transformed with the ligation mixture and plated on LB/ampicillin plates. The resulting colonies were screened by PCR, and positive colonies were grown and their plasmids purified using a Qiagen miniprep. Presence of the correct gene was confirmed by restriction analysis with *Nde*I and *Sma*I (an isoschizimer of *Xma*I). Correct gene sequence of the inserted gene was then confirmed by sequencing. Expression of the gene followed by cleavage of the intein purification tag left Bna7p with an additional Pro-Gly on its C-terminus, and Bna3p with an additional Ala-Gly-His on its N-terminus.

*Protein Expression and Purification.* The pTYB12-BNA3 plasmid was used to transform BL21*CP *E. coli* cells, and the pTYB2-BNA7 plasmid was used to transform ER2566 *E. coli* cells. Six liters of cells were grown in LB medium and 100 $\mu$g/mL ampicillin and induced with 500 $\mu$M IPTG for 16 h at 15 °C when $OD_{600}$ reached 0.5. Cells were harvested, resuspended in IMPACT buffer (20 mM Tris-HCl, pH 8.0, 500 mM NaCl, 1 mM EDTA) containing 0.1% Triton X-100 (and 50 $\mu$M PLP for Bna3 expression), and lysed using a microfluidizer. The lysate was clarified and loaded onto an approximately 15 mL chitin column at 4 °C. Following protein loading, the column was washed with more than 20 column volumes of IMPACT buffer with 0.1% Triton X-100 (with 50 $\mu$M PLP for Bna3 expression) and then washed with IMPACT buffer without Triton (and with 50 $\mu$M PLP for Bna3 expression) until all the Triton X-100 had been removed, as determined by $OD_{280}$. 100 $\mu$L of $\beta$-mercaptoethanol was directly added to the column to initiate thiol cleavage. After 3 days at 4 °C for Bna3p and overnight for Bna7p, the protein was eluted and concentrated with a 10,000 MWCO concentrator, and desalted by 3 buffer exchanges with at least 10 volumes of buffer (10 mM Tris, pH 8.0, 50 mM NaCl, 14 mM mercaptoethanol, 25 $\mu$M PLP for Bna3p, and 10 mM Tris, pH 7.8, 150 mM NaCl for Bna7p).

*Crystallization and Structure Determination of Bna3p.* Bna3p in 10 mM Tris, pH 8.0, 50 mM NaCl, 14 mM mercaptoethanol, 25 $\mu$M PLP was concentrated to an approximate $OD_{280}$ of 40. Crystals were formed using the hanging drop method, using 1 $\mu$L of protein mixed with 2 $\mu$L of well buffer, consisting of 200 mM ammonium nitrate and 24% PEG 1000. Crystals were harvested and transferred to a cryoprotectant consisting of 20% ethylene glycol, 24% PEG 1000 and 200 mM ammonium nitrate and then frozen in liquid nitrogen. Data were collected at the Stanford Synchrotron Radiation Laboratory, beamline 1-5. A space-group of $P2_1$ was determined with unit cell dimensions of $a = 55.78$ Å, $b = 66.52$ Å, $c = 115.20$ Å, $\beta = 90.75°$. Indexing, integration and scaling of reflection data were carried out using HKL2000 to produce a 2.0 Å dataset used for refinement (*45*). The Matthew's coefficient of 2.9 Å$^3$/dalton indicated that there are two molecules per asymmetric unit.

Molecular replacement, using Phaser (*46*), with human kynurenine aminotransferase (PDB accession 1W7L) (*25*) (29% identity and 46% similarity to Bna3p, as calculated by the AlignX module of Vector NTI Suite 9 software from Invitrogen) as a search model, gave a solution that was used as an initial model. Using this model as a starting point, multiple rounds of model building by hand using the program Coot (*47*), with composite omit, and sigma weighted $2F_o - F_c$ and $F_o - F_c$ maps as a guide to correct amino acid placement, and positional refinement, energy minimization and *B*-factor refinement using CNS (*48*) and Refmac (*49*, *50*) were carried out.

Model building brought $R_{free}$ to approximately 30%, at which point the PLP was clearly visible in both $F_o - F_c$ and $2F_o - F_c$ maps. Libraries for LLP were generated using the PRODRG server (http://davapc1.bioch.dundee.ac.uk/programs/

prodrg/prodrg.html) (*51*) and modified to reflect atom naming as used in PDB entry 1W7L. Libraries for NFK and KYN models were also generated using the PRODRG server.

Geometry and side chain placement were adjusted by hand. Water molecules were added automatically, using Coot software, and then checked manually. The final model had an $R_{cryst}$ of 22.8% and an $R_{free}$ of 27.1% and contained 849 amino acids (including the PLP attached to Lys271 as an internal aldimine) and 242 water molecules. In both monomers the first 20 residues (including the 3 added from the cloning process) had no visible electron density and were not modeled in. Additionally, residues 48−51 of the A chain and 49 and 50 of the B chain had no interpretable electron density and were not modeled. Ramachandran statistics were calculated using the program Procheck (*52*). Diffraction-component precision index (DPI) was calculated using the program SFCHECK (*53*). All figures were generated using the program PyMol (DeLano, W. L., The PyMOL Molecular Graphics System (2002) DeLano Scientific, San Carlos, CA).

*Enzyme Assays. KAT Activity Assay*. Bna3p was diluted to 200 $\mu$g/mL in 100 mM Tris, pH 8.5, 25 $\mu$M PLP, and between 1 and 20 mM α-keto acid (final concentration). The reaction was started by adding substrate (generally 0.5 to 6 mM) and was carried out at 37 °C in a 1 mL volume in a heated quartz cuvette. The velocity was constant for at least the first 30 min at all substrate concentrations, and the reaction was run for 20 min to calculate a rate. A continuous assay was developed in which KA production was determined by measuring the increase in $OD_{285}$ over time. This reduced the variability we found when we used an assay in which the reaction was stopped by addition of an acid and the protein removed by centrifugation. However, both KA and KYN have significant absorbance at 285 nm. Thus the loss of KYN had a substantial effect on $OD_{285}$. Furthermore, the $OD_{285}$ for KYN was not linear with KYN concentration at the higher concentrations used in this assay. To account for these, a standard curve was generated for each concentration of KYN substrate used. This was done by mixing between 0 and 100 $\mu$M KA with KYN and keeping the total concentration of KA + KYN constant (since one molecule of KYN is converted to one molecule of KA) for each of the substrate concentrations. This generated 6 sets of concentration of KA vs $OD_{285}$ curves, each of which was linear, but each of which had a different slope (in ΔAU/mM) (Presumably the differing slopes are due to the nonlinearity of $OD_{285}$ vs concentration of KYN at high concentrations). Change in $OD_{285}$ was measured over time and a rate (ΔAU/h) was calculated. This rate was then divided by the ΔAU/mM for the given substrate concentration to produce a rate in mM/hr.

*FKF Activity Assay*. NFK was added to 0.1% BSA, 50 mM potassium phosphate, pH 7.3 at final concentrations of between 1 mM and 31 $\mu$M. The reaction (carried out in a 150 $\mu$L volume) was initiated by addition of Bna7p to a final concentration of 14 ng/mL, and formation of kynurenine was determined by measuring the increase in $OD_{360}$, using a quartz microcuvette (100 $\mu$L minimum volume). Because NFK absorbs slightly at 360 nm (about 10% of the value of kynurenine at the same wavelength), measured ODs were adjusted by increasing the measured OD by 11% to account for the loss of $OD_{360}$ from the loss of substrate. After the adjustment, the rate of increase of $OD_{360}$ was converted to concentration of KYN by using an extinction coefficient of 4,200 $cm^{-1}$ $M^{-1}$, which was determined using commercially available KYN as a standard. Kinetic parameters $k_{cat}$ and $K_m$ were determined by fitting the experimental results to the Michaelis−Menten equation using the program KaleidaGraph 3.0. Averages of velocities from 6 separate experiments were used. Enzyme concentrations for both enzymes were determined by Bradford assay using BSA as a standard.

*Metabolite Extraction and Measurement.* Extraction of metabolites was based on previously published methods (*36*, *54*). Yeast strains were grown overnight at 30 °C in YPD. They were diluted into 100 mL of fresh YPD to approximately $OD_{600}$ of 0.2 and then grown to $OD_{600}$ of 1.8. All 100 mL of cells was spun down (10 min at 10000*g*) and resuspended in ice cold PBS (150 mM NaCl, 50 mM potassium phosphate, pH 7.3). Cells were again spun down and resuspended in 2 mL of ice cold MilliQ water. The resulting suspension was aliquotted at 250 $\mu$L per tube into ten 1.5 mL tubes on ice. 250 $\mu$L of −20 °C methanol was then added to each tube, and the tubes were put on dry ice for 30 min. Samples were then thawed on ice for 10 min before being centrifuged at 4 °C for 10 min at 16000*g*. Supernatants were then pooled, and pellets were washed in 500 $\mu$L of ice cold methanol, which was then added to the original supernatants. The resulting extract (around 10 mL) was then concentrated to 100 $\mu$L using a SpeedVac. 5 $\mu$L of this sample was injected for analysis by LC−MS.

LC−MS measurements were done at the University of California Davis Metabolomics core facility. Measurements of tryptophan metabolites were done similarly to those previously described (*55*, *56*), except that the method was modified for a short (5 min) LC run on a 4 × 50 mm C18 column, 3 $\mu$m particle size. The LC run was isocratic, using 5% acetonitrile, 95% 5 mM ammonium acetate, pH 5.5 buffer. The detector was an ion trap mass spectrometer (Finnigan LTQ) equipped with an electrospray ion source. Detection was done in positive mode applying selective reaction monitoring scan (SRM). Commercially available KYN, KA, quinaldic acid and 3-hydroxykynurenine were used as standards. For NFK measurements, the mixture of NFK and NAK was added as a standard, and each of the two compounds was individually detected as a standard.

*Growth Rate Measurement.* The same strains used for metabolite extraction were used to measure growth rates in the presence or absence of nicotinate. Yeast cultures were grown overnight at 30 °C in liquid YPD. Cells were washed 2 times with SD media with no nicotinate (niacin) (*57*), but supplemented with 20 mg/L of uracil, L-histidine HCl, L-leucine, and L-lysine HCl. $OD_{600}$ was determined for each culture, and 40 mL of above-described SD medium was inoculated to an $OD_{600}$ of 0.1. Cultures were then grown for 24 h at 30 °C in order to deplete any stores of $NAD^+$. 80 mL of of above-described SD medium was inoculated to an $OD_{600}$ of 0.2. This was then split into 2 40 mL cultures in 250 mL Erlenmeyer flasks, one of which was then supplemented with nicotinate at a final concentration of 0.5 mg/L. Cultures were returned to 30 °C and incubated with shaking. 1 mL samples were periodically taken, and $OD_{600}$ was measured on a Hewlett-Packard 8452A diode array spectrophotometer. Doubling times were calculated as the inverse slope of a straight line fitted to a $Log_2(OD_{600})$ vs time plot. All $R^2$ values for the linear curve fits were at least 0.99.

## SUPPORTING INFORMATION AVAILABLE

Graph of Vi versus kynurenine concentration for Bna3p (Figure S1). This material is available free of charge via the Internet at http://pubs.acs.org.

## REFERENCES


1. Lehman, I. R., Bessman, M. J., Simms, E. S., and Kornberg, A. (1958) Enzymatic synthesis of deoxyribonucleic acid. I. Preparation of substrates and partial purification of an enzyme from Escherichia coli, *J. Biol. Chem. 233*, 163−170.
2. Olivera, B. M., and Lehman, I. R. (1967) Diphosphopyridine nucleotide: a cofactor for the polynucleotide-joining enzyme from Escherichia coli, *Proc. Natl. Acad. Sci. U.S.A. 57*, 1700−1704.
3. Imai, S., Armstrong, C. M., Kaeberlein, M., and Guarente, L. (2000) Transcriptional silencing and longevity protein Sir2 is an NAD-dependent histone deacetylase, *Nature 403*, 795−800.
4. Lin, S. J., Defossez, P. A., and Guarente, L. (2000) Requirement of NAD and SIR2 for life-span extension by calorie restriction in Saccharomyces cerevisiae, *Science 289*, 2126−2128.
5. Wilkinson, A., Day, J., and Bowater, R. (2001) Bacterial DNA ligases, *Mol. Microbiol. 40*, 1241−1248.
6. Belenky, P., Bogan, K. L., and Brenner, C. (2007) NAD+ metabolism in health and disease, *Trends Biochem. Sci. 32*, 12−19.
7. Luo, J., Nikolaev, A. Y., Imai, S., Chen, D., Su, F., Shiloh, A., Guarente, L., and Gu, W. (2001) Negative control of p53 by Sir2alpha promotes cell survival under stress, *Cell 107*, 137−148.
8. Panozzo, C., Nawara, M., Suski, C., Kucharczyka, R., Skoneczny, M., Becam, A. M., Rytka, J., and Herbert, C. J. (2002) Aerobic and anaerobic NAD+ metabolism in Saccharomyces cerevisiae, *FEBS Lett. 517*, 97−102.
9. Stone, T. W. (2001) Kynurenines in the CNS: from endogenous obscurity to therapeutic importance, *Prog Neurobiol. 64*, 185−218.
10. Stone, T. W. (2000) Inhibitors of the kynurenine pathway, *Eur. J. Med. Chem. 35*, 179−186.
11. Stone, T. W., and Darlington, L. G. (2002) Endogenous kynurenines as targets for drug discovery and development, *Nat. Rev. Drug Discovery 1*, 609−620.
12. Kwok, J. B., Kapoor, R., Gotoda, T., Iwamoto, Y., Iizuka, Y., Yamada, N., Isaacs, K. E., Kushwaha, V. V., Church, W. B., Schofield, P. R., and Kapoor, V. (2002) A missense mutation in kynurenine aminotransferase-1 in spontaneously hypertensive rats, *J. Biol. Chem. 277*, 35779−35782.
13. Jansonius, J. N. (1998) Structure, evolution and action of vitamin B6-dependent enzymes, *Curr. Opin. Struct. Biol. 8*, 759−769.
14. Baran, H., Okuno, E., Kido, R., and Schwarcz, R. (1994) Purification and characterization of kynurenine aminotransferase I from human brain, *J. Neurochem. 62*, 730−738.
15. Alberati-Giani, D., Malherbe, P., Kohler, C., Lang, G., Kiefer, V., Lahm, H. W., and Cesura, A. M. (1995) Cloning and characterization of a soluble kynurenine aminotransferase from rat brain: identity with kidney cysteine conjugate beta-lyase, *J. Neurochem. 64*, 1448−1455.
16. Goto, M., Omi, R., Miyahara, I., Hosono, A., Mizuguchi, H., Hayashi, H., Kagamiyama, H., and Hirotsu, K. (2004) Crystal structures of glutamine:phenylpyruvate aminotransferase from Thermus thermophilus HB8: induced fit and substrate recognition, *J. Biol. Chem. 279*, 16518−16525.
17. Han, Q., and Li, J. (2004) Cysteine and keto acids modulate mosquito kynurenine aminotransferase catalyzed kynurenic acid production, *FEBS Lett. 577*, 381−385.
18. Han, Q., Li, J., and Li, J. (2004) pH dependence, substrate specificity and inhibition of human kynurenine aminotransferase I, *Eur. J. Biochem. 271*, 4804−4814.
19. Kucharczyk, R., Zagulski, M., Rytka, J., and Herbert, C. J. (1998) The yeast gene YJR025c encodes a 3-hydroxyanthranilic acid dioxygenase and is involved in nicotinic acid biosynthesis, *FEBS Lett. 424*, 127−130.
20. Bedalov, A., Hirao, M., Posakony, J., Nelson, M., and Simon, J. A. (2003) NAD+-dependent deacetylase Hst1p controls biosynthesis and cellular NAD+ levels in Saccharomyces cerevisiae, *Mol. Cell. Biol. 23*, 7044−7054.
21. Arndt, J. W., Schwarzenbacher, R., Page, R., Abdubek, P., Ambing, E., Biorac, T., Canaves, J. M., Chiu, H. J., Dai, X., Deacon, A. M., DiDonato, M., Elsliger, M. A., Godzik, A., Grittini, C., Grzechnik, S. K., Hale, J., Hampton, E., Han, G. W., Haugen, J., Hornsby, M., Klock, H. E., Koesema, E., Kreusch, A., Kuhn, P., Jaroszewski, L., Lesley, S. A., Levin, I., McMullan, D., McPhillips, T. M., Miller, M. D., Morse, A., Moy, K., Nigoghossian, E., Ouyang, J., Peti, W. S., Quijano, K., Reyes, R., Sims, E., Spraggon, G., Stevens, R. C., van den Bedem, H., Velasquez, J., Vincent, J., von Delft, F., Wang, X., West, B., White, A., Wolf, G., Xu, Q., Zagnitko, O., Hodgson, K. O., Wooley, J., and Wilson, I. A. (2005) Crystal structure of an alpha/beta serine hydrolase (YDR428C) from Saccharomyces cerevisiae at 1.85 Å resolution, *Proteins 58*, 755−758.
22. Pabarcus, M. K., and Casida, J. E. (2002) Kynurenine formamidase: determination of primary structure and modeling-based prediction of tertiary structure and catalytic triad, *Biochim. Biophys. Acta 1596*, 201−211.
23. Pabarcus, M. K., and Casida, J. E. (2005) Cloning, expression, and catalytic triad of recombinant arylformamidase, *Protein Expression Purif. 44*, 39−44.
24. Altschul, S. F., Madden, T. L., Schaffer, A. A., Zhang, J., Zhang, Z., Miller, W., and Lipman, D. J. (1997) Gapped BLAST and PSI-BLAST: a new generation of protein database search programs, *Nucleic Acids Res. 25*, 3389−3402.
25. Rossi, F., Han, Q., Li, J., Li, J., and Rizzi, M. (2004) Crystal structure of human kynurenine aminotransferase I, *J. Biol. Chem. 279*, 50214−50220.
26. Han, Q., Gao, Y. G., Robinson, H., Ding, H., Wilson, S., and Li, J. (2005) Crystal structures of Aedes aegypti kynurenine aminotransferase, *Febs. J. 272*, 2198−2206.
27. Hosono, A., Mizuguchi, H., Hayashi, H., Goto, M., Miyahara, I., Hirotsu, K., and Kagamiyama, H. (2003) Glutamine:phenylpyruvate aminotransferase from an extremely thermophilic bacterium, Thermus thermophilus HB8, *J. Biochem. (Tokyo) 34*, 843−851.
28. Nakai, T., Okada, K., Akutsu, S., Miyahara, I., Kawaguchi, S., Kato, R., Kuramitsu, S., and Hirotsu, K. (1999) Structure of Thermus thermophilus HB8 aspartate aminotransferase and its complex with maleate, *Biochemistry 38*, 2413−2424.
29. Chon, H., Matsumura, H., Koga, Y., Takano, K., and Kanaya, S. (2005) Crystal structure of a human kynurenine aminotransferase II homologue from Pyrococcus horikoshii OT3 at 2.20 A resolution, *Proteins 61*, 685−688.
30. Holm, L., and Sander, C. (1996) Mapping the protein universe, *Science 273*, 595−603.
31. Holm, L., and Park, J. (2000) DaliLite workbench for protein structure comparison, *Bioinformatics 16*, 566−567.
32. Gish, W., and States, D. J. (1993) Identification of protein coding regions by database similarity search, *Nat. Genet. 3*, 266−272.
33. Stoldt, V., Rademacher, F., Kehren, V., Ernst, J. F., Pearce, D. A., and Sherman, F. (1996) Review: the Cct eukaryotic chaperonin subunits of Saccharomyces cerevisiae and other yeasts, *Yeast 12*, 523−529.
34. Heikinheimo, P., Goldman, A., Jeffries, C., and Ollis, D. L. (1999) Of barn owls and bankers: a lush variety of alpha/beta hydrolases, *Structure 7*, R141−146.
35. Pan, X., Ye, P., Yuan, D. S., Wang, X., Bader, J. S., and Boeke, J. D. (2006) A DNA integrity network in the yeast Saccharomyces cerevisiae, *Cell 124*, 1069−1081.
36. Maharjan, R. P., and Ferenci, T. (2003) Global metabolite analysis: the influence of extraction methodology on metabolome profiles of Escherichia coli, *Anal. Biochem. 313*, 145−154.
37. Bencharit, S., Morton, C. L., Howard-Williams, E. L., Danks, M. K., Potter, P. M., and Redinbo, M. R. (2002) Structural insights into CPT-11 activation by mammalian carboxylesterases, *Nat. Struct. Biol. 9*, 337−342.
38. Wheelock, C. E., Colvin, M. E., Uemura, I., Olmstead, M. M., Sanborn, J. R., Nakagawa, Y., Jones, A. D., and Hammock, B. D. (2002) Use of *ab initio* calculations to predict the biological potency of carboxylesterase inhibitors, *J. Med. Chem. 45*, 5576−5593.
39. Daniel, J. A., Keyes, B. E., Ng, Y. P., Freeman, C. O., and Burke, D. J. (2006) Diverse functions of spindle assembly checkpoint genes in Saccharomyces cerevisiae, *Genetics 172*, 53−65.
40. Okuno, E., Nakamura, M., and Schwarcz, R. (1991) Two kynurenine aminotransferases in human brain, *Brain Res. 542*, 307−312.
41. Guidetti, P., Okuno, E., and Schwarcz, R. (1997) Characterization of rat brain kynurenine aminotransferases I and II, *J. Neurosci. Res. 50*, 457−465.

42. Urrestarazu, A., Vissers, S., Iraqui, I., and Grenson, M. (1998) Phenylalanine- and tyrosine-auxotrophic mutants of Saccharomyces cerevisiae impaired in transamination, *Mol. Gen. Genet. 257*, 230−237.
43. Schoondermark-Stolk, S. A., Jansen, M., Veurink, J. H., Verkleij, A. J., Verrips, C. T., Euverink, G. J., Boonstra, J., and Dijkhuizen, L. (2006) Rapid identification of target genes for 3-methyl-1-butanol production in Saccharomyces cerevisiae, *Appl. Microbiol. Biotechnol. 70*, 237−246.
44. Kurnasov, O., Jablonski, L., Polanuyer, B., Dorrestein, P., Begley, T., and Osterman, A. (2003) Aerobic tryptophan degradation pathway in bacteria: novel kynurenine formamidase, *FEMS Microbiol. Lett. 227*, 219−227.
45. Otwinowski, Z., and Minor, W. (1997) *Processing of X-ray Diffraction Data Collected in Oscillation Mode*, Vol. 276, Academic Press, New York.
46. Storoni, L. C., McCoy, A. J., and Read, R. J. (2004) Likelihood-enhanced fast rotation functions, *Acta Crystallogr., Sect. D: Biol. Crystallogr. 60*, 432−438.
47. Emsley, P., and Cowtan, K. (2004) Coot: model-building tools for molecular graphics, *Acta Crystallogr., Sect. D: Biol. Crystallogr. 60*, 2126−2132.
48. Brunger, A. T., Adams, P. D., Clore, G. M., DeLano, W. L., Gros, P., Grosse-Kunstleve, R. W., Jiang, J. S., Kuszewski, J., Nilges, M., Pannu, N. S., Read, R. J., Rice, L. M., Simonson, T., and Warren, G. L. (1998) Crystallography & NMR system: A new software suite for macromolecular structure determination, *Acta Crystallogr., Sect. D: Biol. Crystallogr. 54* (Part 5), 905−921.
49. Collaborative Computational Project-Number 4 (1994) The CCP4 suite: programs for protein crystallography, *Acta Crystallogr., Sect. D: Biol. Crystallogr. 50*, 760−763.
50. Murshudov, G. N., Vagin, A. A., and Dodson, E. J. (1997) Refinement of macromolecular structures by the maximum-likelihood method, *Acta Crystallogr., Sect. D: Biol. Crystallogr. 53*, 240−255.
51. van Aalten, D. M., Bywater, R., Findlay, J. B., Hendlich, M., Hooft, R. W., and Vriend, G. (1996) PRODRG, a program for generating molecular topologies and unique molecular descriptors from coordinates of small molecules, *J. Comput.-Aided Mol. Des. 10*, 255−262.
52. Laskowski, R. A., MacArthur, M. W., Moss, D. S., and Thornton, J. M. (1993) PROCHECK: a program to check the stereochemical quality of protein structures, *J. Appl. Crystallogr. 26*, 283−291.
53. Vaguine, A. A., Richelle, J., and Wodak, S. J. (1999) SFCHECK: a unified set of procedures for evaluating the quality of macromolecular structure-factor data and their agreement with the atomic model, *Acta Crystallogr., Sect. D: Biol. Crystallogr. 55*, 191−205.
54. Villas-Boas, S. G., Hojer-Pedersen, J., Akesson, M., Smedsgaard, J., and Nielsen, J. (2005) Global metabolite analysis of yeast: evaluation of sample preparation methods, *Yeast 22*, 1155−1169.
55. Amirkhani, A., Heldin, E., Markides, K. E., and Bergquist, J. (2002) Quantitation of tryptophan, kynurenine and kynurenic acid in human plasma by capillary liquid chromatography-electrospray ionization tandem mass spectrometry, *J. Chromatogr., B: Anal. Technol. Biomed. Life Sci. 780*, 381−387.
56. Maneglier, B., Rogez-Kreuz, C., Cordonnier, P., Therond, P., Advenier, C., Dormont, D., Clayette, P., and Spreux-Varoquaux, O. (2004) Simultaneous measurement of kynurenine and tryptophan in human plasma and supernatants of cultured human cells by HPLC with coulometric detection, *Clin. Chem. 50*, 2166−2168.
57. Sherman, F. (1991) Getting started with yeast. *Methods Enzymol. 194*, 3−21.

BI701172V